ACS OMEGA

http://pubs.acs.org/journal/acsodf

Article

Generation Characteristics of Solid Byproducts of the $C_4F_7N-CO_2-O_2$ Gas Mixture under PD Fault

Ran Zhuo, Mingli Fu, Dibo Wang,* Yan Luo, Guoli Wang, and Lei Jia

Cite This: *ACS Omega* 2023, 8, 23457−23464

Read Online

ACCESS | Metrics & More | Article Recommendations

ABSTRACT: With the gradual improvement of the requirements for the safe and stable operation of gas-insulated equipment (GIE), the eco-friendly insulating gas $C_4F_7N-CO_2-O_2$ has become the best choice to replace SF_6 and apply it to various medium-voltage (MV) and high-voltage (HV) GIE. At present, the generation characteristics of solid decomposition products of the $C_4F_7N-CO_2-O_2$ gas mixture under partial discharge (PD) fault need to be studied. In this paper, a 96 h PD decomposition test was carried out by simulating metal protrusion defects in GIE with needle-plate electrodes to study the generation characteristics of $C_4F_7N-CO_2-O_2$ gas mixture solid decomposition products under PD fault and their compatibility with metal conductors. It was found that obvious ring-shaped solid precipitates appeared in the central area of the surface of the plate electrode under the action of long-term PD, mainly including metal oxides (CuO), silicates ($CuSiO_3$), fluorides (CuF, CF_X), carbon oxides (CO, CO_2), and nitrogen oxides (NO, NO_2). The addition of 4% O_2 has little effect on the element composition and valence state of PD solid precipitates, but it can reduce their yield to a certain extent. The corrosion effect of O_2 in the gas mixture on metal conductors is weaker than that of C_4F_7N.

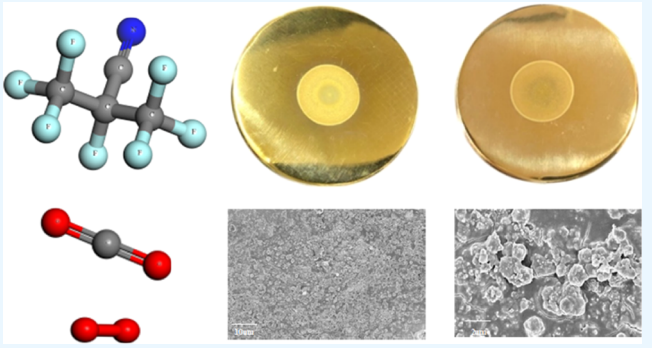

1. INTRODUCTION

Sulfur hexafluoride (SF_6) is widely used in various gas-insulated transmission and distribution equipment as an ideal insulating and arc-extinguishing dielectric.[1−3] However, the potential value of the greenhouse effect of SF_6 is 23,500 times that of CO_2, and the atmospheric life is 3200 years, which is a very strong greenhouse effect gas.[4,5] Looking for eco-friendly gas insulating media that can be applied to various medium- and high-voltage GIE can fundamentally solve the dependence of the power industry on the large use of SF_6 gas.[6,7] In recent years, perfluoroisobutyronitrile (C_4F_7N) gas mixture is considered a potential SF_6 substitute gas due to its excellent environmental protection and insulation performance.[8−10]

The decomposition of fluorocarbon gas under different types of electrical and thermal faults will not only generate gas byproducts but also generate some solid byproducts. During the breaking process, carbon particles precipitated by the decomposition of fluorocarbon gas under the action of a high-energy arc will attach to the switch contact, affecting the breaking performance,[11] and may also attach to the insulator, causing different degrees of insulation faults. In addition, the decomposition of fluorocarbon gas to generate fluoride under long-term discharge failure will interact with the metal guide rods in the equipment to generate solid compounds that affect the conductivity. Therefore, it is of great significance for the safe and stable operation of the equipment to study the generation law of solid byproducts and gas−solid compatibility of the C_4F_7N gas mixture under discharge fault.

At present, certain achievements have been made in the research of solid byproducts of the C_4F_7N gas mixture under different types of electrical and thermal faults. Meyer et al. pointed out that adding a certain amount of O_2 into the $C_4F_7N-CO_2$ gas mixture can avoid carbon deposition on the insulator and the formation of some fluoride, thus improving the breaking performance of the gas mixture.[12] Li et al. carried out 2000 alternating current (AC) breakdown tests on the $C_4F_7N-CO_2$ gas mixture and found that a layer of light-yellow solid powder would be attached to the gas chamber wall and the electrode surface after the test. The scanning electron microscope (SEM) analysis showed that the solid byproducts were irregular shapes ranging from hundreds of nanometers to tens of nanometers in size, and the energy-dispersive spectrometer (EDS) analysis showed that the solid byproducts were composed of several elements like Cu, N, F, and Si. The

Received: January 17, 2023
Accepted: March 31, 2023
Published: June 20, 2023

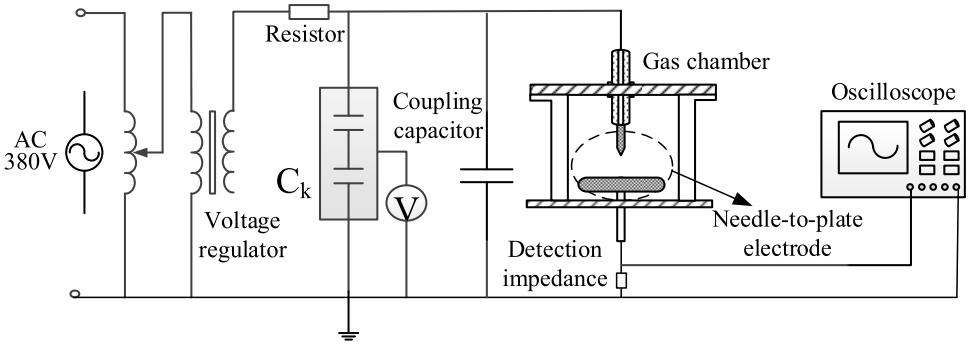

Figure 1. Schematic diagram of the PD decomposition test platform.

gas byproducts may react with the brass electrode to produce copper fluoride and copper cyanide.[13] Zhang et al. carried out 150 AC breakdown tests of a 6% C_4F_7N−94% N_2 gas mixture and found that some black solid material (carbon) appeared on the surface of the ball electrode after the test. The conductive property of carbon particles would affect the insulation strength of the gas mixture, and the addition of O_2 could significantly inhibit the generation of black solid material on the electrode surface. The conductivity of carbon particles would affect the insulation strength of the gas mixture, while the addition of O_2 could significantly inhibit the generation of carbon particles.[14] Han et al. found that a layer of yellow-brown solid powder was attached to the inner wall of the stainless-steel gas chamber after the thermal decomposition (6 h, 700 °C) test of the C_4F_7N−CO_2 gas mixture, which was mainly F and Fe according to EDS test analysis.[15]

In general, the decomposition of the C_4F_7N gas mixture under arc breaking, power frequency breakdown, and overheating faults will generate solid byproducts, but the composition and content of byproducts will vary under different fault conditions and different test conditions. PD fault is one of the most common faults of GIE. The cumulative effect of energy generated by long-term weak discharge will gradually degrade the dielectric properties of the insulating medium and decompose, generating a series of gas and solid byproducts.[16−18] At present, there are few studies on the solid byproducts of the C_4F_7N gas mixture under PD fault. Although the addition of O_2 can bring some advantages to the chemical stability of the C_4F_7N−CO_2 mixture, due to the strong oxidation of O_2, the generation characteristics of solid byproducts of the C_4F_7N−CO_2 gas mixture after the addition of O_2 under PD fault and its gas−solid compatibility with metal conductors need further study.

In this paper, a 96 h PD decomposition test of the C_4F_7N−CO_2−O_2 gas mixture at 0% O_2 and 4% O_2 was carried out by using a needle-plate electrode to simulate the defects of metal protrusions in the GIE. The microscopic morphology, element composition, content, and valence of the solid precipitate area on the surface of the electrode after the test were characterized based on SEM, EDS, and X-ray photoelectron spectroscopy (XPS), and the generation characteristics and the influence of O_2 on its generation were analyzed. Finally, the gas−solid compatibility of the C_4F_7N−CO_2−O_2 gas mixture and the metal conductor in the equipment under PD fault is evaluated, and its engineering application suggestions are given based on the test and analysis results.

2. EXPERIMENT SETUP AND METHOD

Figure 1 shows the PD fault decomposition characteristic test system. The AC high voltage generated by the test transformer is applied to the insulation defect through the current limiting resistance (10 kΩ). The capacitive voltage divider (500 pF/500 nF) is used to measure the AC high voltage provided by the transformer. Based on the pulse current method recommended by the IEC60270 standard, the coupling capacitance and noninductive detection impedance are used to measure the pulse signal of PD.[19] A high-speed digital storage oscilloscope (Tektronix DPO7104) is used to collect PD signals. The gas chamber is a self-made stainless-steel tank with a volume of about 29 L, which can withstand a pressure of 1 MPa at most and has good sealing performance. In the test, the pin-plate electrode is used to simulate the extremely uneven electric field. The pin-plate electrode spacing is set at 10 mm, and the material is brass. The radius of curvature of the needle tip is 0.3 mm, the diameter of the plate electrode is 70 mm, and the thickness is 8 mm.

Before the test, the wall of the gas chamber was cleaned with anhydrous alcohol, and the airtightness of the device was tested after drying. Then, the gas chamber was vacuumized and filled with CO_2 (purity 99.999%) three times to remove the possible impact of impure gas on the test results. Finally, the C_4F_7N−CO_2−O_2 gas mixture with a fixed mixing ratio was filled for the test.

At present, the inflation pressure of MV GIE is generally not more than 0.20 MPa. Previous research indicates that if the C_4F_7N−CO_2 gas mixture is required to meet the minimum operating temperature of −25 °C within the pressure range of 0.1−0.2 MPa, the content of C_4F_7N in the mixture should not exceed 18%.[20] In addition, research shows that the generation of most of the decomposition products of the C_4F_7N−CO_2−O_2 gas mixture is the lowest at 4% O_2 after the 96 h PD decomposition test,[21] so this paper studies the generation characteristics of the solid decomposition products of the C_4F_7N−CO_2−O_2 gas mixture containing 15% C_4F_7N at 0.14 MPa under different O_2 contents (0 and 4%), and the discharge time of each group of tests is 96 h. The gas and solid byproducts of the C_4F_7N−CO_2−O_2 gas mixture at different O_2 contents were analyzed and tested based on GC-MS, SEM, EDS, and XPS, and the gas−solid compatibility of the mixture and metal conductor at different O_2 contents was evaluated based on the relevant results.

3. RESULTS AND DISCUSSION

3.1. PD Gaseous Byproducts of the C_4F_7N−CO_2−O_2 Gas Mixture. During the 96 h PD test, the gas in the stainless-

https://doi.org/10.1021/acsomega.3c00345
ACS Omega 2023, 8, 23457−23464

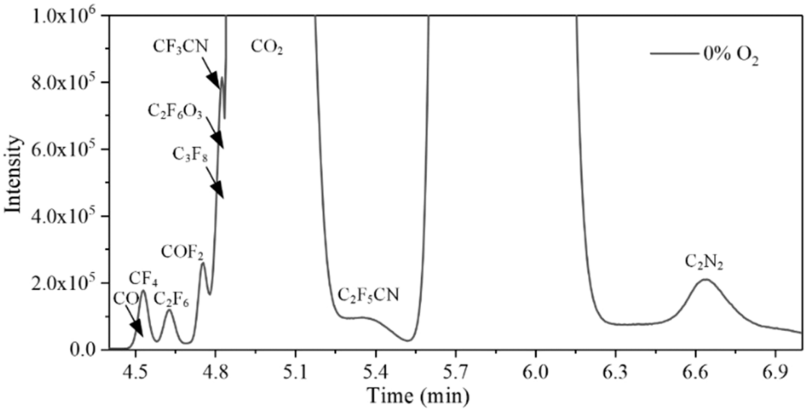

Figure 2. Gas chromatogram of the C_4F_7N−CO_2 gas mixture after the 96 h PD test.

steel gas chamber is collected every 12 h for composition analysis. Considering that the gas composition in the gas chamber tends to be stable at the end of the test, this paper only analyzes the gas composition of 96 h. Figure 2 shows the gas chromatogram of the 15% C_4F_7N−85% CO_2 gas mixture after the 96 h PD test. From the characteristic peak in the figure, it can be seen that the main products of the C_4F_7N−CO_2 gas mixture PD decomposition are CF_4, C_2F_6, C_3F_8, C_3F_6, CO, COF_2, $C_2F_6O_3$, CF_3CN, C_2F_5CN, and C_2N_2. Based on the qualitative analysis of gas decomposition products, it is found that the type of gas decomposition products will not change significantly after adding O_2 into the C_4F_7N−CO_2 mixture.

In this paper, CF_4, C_2F_6, C_3F_8, C_3F_6, and CO, five decomposition products with standard gases, are detected and analyzed by using the external standard method. Figure 3

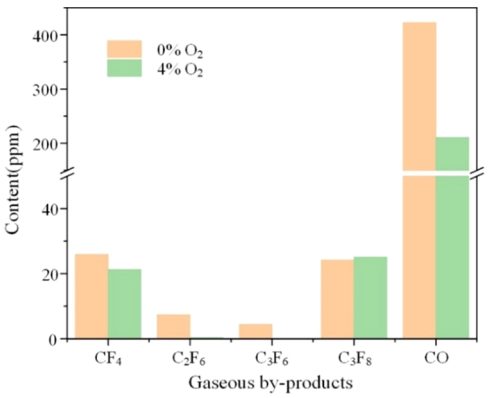

Figure 3. Production of some gas byproducts with different O_2 contents.

shows the yield of quantifiable gas byproducts after 96 h PD of the C_4F_7N−CO_2−O_2 gas mixture containing 0% O_2 and 4% O_2. It can be seen that the yield of other byproducts decreased to varying degrees after the addition of 4% O_2; except for the slight increase of C_3F_8, the yields of C_2F_6 and C_3F_6 decreased to 0 ppm after the addition of 4% O_2, indicating that the addition of 4% O_2 can significantly inhibit the production of these two byproducts.

3.2. PD Solid Byproduct of the C_4F_7N−CO_2−O_2 Gas Mixture. *3.2.1. Macroscopic and Microscopic Morphologies.* After the 96 h PD decomposition test of the C_4F_7N−CO_2−O_2 gas mixture, the corrosion phenomenon on the surface of the plate electrode was observed, which was mainly caused by a ring of solid precipitates. Figure 4 shows the macro morphology of the electrode surface before and after the PD test. It can be seen that compared with the electrode before the test, there are more obvious ring-shaped solid precipitates in the central area of the electrode surface after the test, and the color becomes darker the closer they get to the electrode center. This phenomenon indicates that the C_4F_7N−CO_2−O_2 gas mixture will generate solid precipitates and cause corrosion to the plate electrode under the long-term PD condition.

In order to further explore the interaction characteristics of the C_4F_7N−CO_2−O_2 gas mixture with the copper electrode under the action of long-time PD and the influence of O_2 on the solid precipitates of the C_4F_7N−CO_2 gas mixture, SEM, EDS, and XPS were used to analyze the micromorphology, element composition, and content of the solid precipitates. Figure 5 shows the SEM of the solid precipitates under different magnifications. It can be found that the surface structure of the copper electrode before the test is flat, and the fine-grained cutting section is clearly visible (Figure 5a), with dense scale corrosion seen on the copper surface after the 96

Figure 4. Macro morphology of the plate electrode before and after the 96 h PD test. (a) Control group. (b) 0% O_2. (c) 4% O_2.

https://doi.org/10.1021/acsomega.3c00345
ACS Omega 2023, 8, 23457−23464

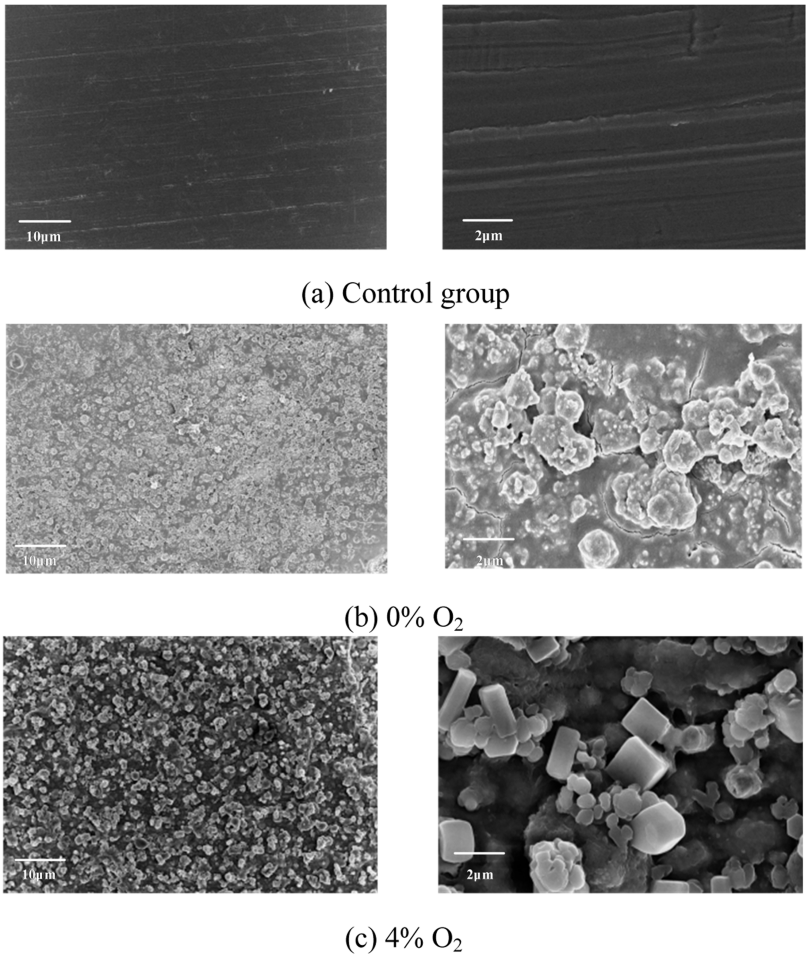

Figure 5. Electrode surface SEM before and after the 96 h PD test. (a) Control group. (b) 0% O_2. (c) 4% O_2.

PD test in the 15% C_4F_7N−85% CO_2 gas mixture (Figure 5b). After adding 4% O_2, it can be seen that spherical and cubic crystalline corrosions are distributed in various areas of the copper surface (Figure 5c). Both of the above cases show that the microstructure of the copper electrode surface has changed significantly, and the particle stratification is shown in the high-magnification image, indicating that the textured cutting section of the copper surface completely disappears and the microstructure of the copper surface is seriously damaged under the long-term PD condition. From the distribution area and distribution density of solid substances, it can be seen that the yield of solid byproducts generated without O_2 is significantly greater than that with 4% O_2, indicating that O_2 may inhibit the generation of solid byproducts while inhibiting gas byproducts.

3.2.2. Component Analysis. EDS is mainly used in conjunction with SEM to select the small position area of the sample and detect its element composition and content. Table 1 shows the qualitative and quantitative analysis results of EDS on the electrode surface after PD. The solid precipitates on the electrode surface are mainly composed of C, N, O, F, and Si, and the Si element mainly comes from the main component SiO_2 in the side observation window of the stainless-steel gas chamber. EDS quantitative analysis results are usually expressed in mass percentage (wt %). The mass percentage of the F element decreased by 26.3% after the addition of 4% O_2 compared with the absence of O_2. F is mainly from fluoride in the solid byproducts generated on the electrode surface, so the distribution area and density of solid substances after adding O_2 are significantly smaller than that without adding O_2. It also further shows that O_2 can inhibit the formation of byproducts to a certain extent.

Table 1. Analysis of EDS Elements on the Electrode Surface after PD

	apparent concentration		wt (%)	
element	0% O_2	4% O_2	0% O_2	4% O_2
C	7.69	8.14	14.91	15.43
N	5.58	7.27	7.03	9.24
O	17.00	18.24	19.25	22.19
F	23.90	15.89	26.49	19.51
Si	3.45	1.95	2.49	1.43
Cu	27.22	30.36	29.83	32.20

In order to further explore the chemical state of the element composition of solid precipitates on the electrode surface after the PD test, five elements of Cu, F, O, N, and C were selected for XPS analysis based on the EDS analysis results. Figure 6 shows the XPS of solid precipitates under 0% O_2 and 4% O_2 conditions. The abscissa of the XPS spectrum is the atomic orbital binding energy (BE), and the ordinate is the peak intensity. The Gaussian method is used for peak fitting. At 0% O_2, Cu is mainly composed of three characteristic peaks at 935.01, 943.95, and 954 eV, corresponding to $CuSiO_3$ $2p_{3/2}$, CuO $2p_{3/2}$, and CuF (Figure 6a). The characteristic peaks of the F element at 684.15 and 688.36 eV correspond to CuF_2

https://doi.org/10.1021/acsomega.3c00345
ACS Omega 2023, 8, 23457−23464

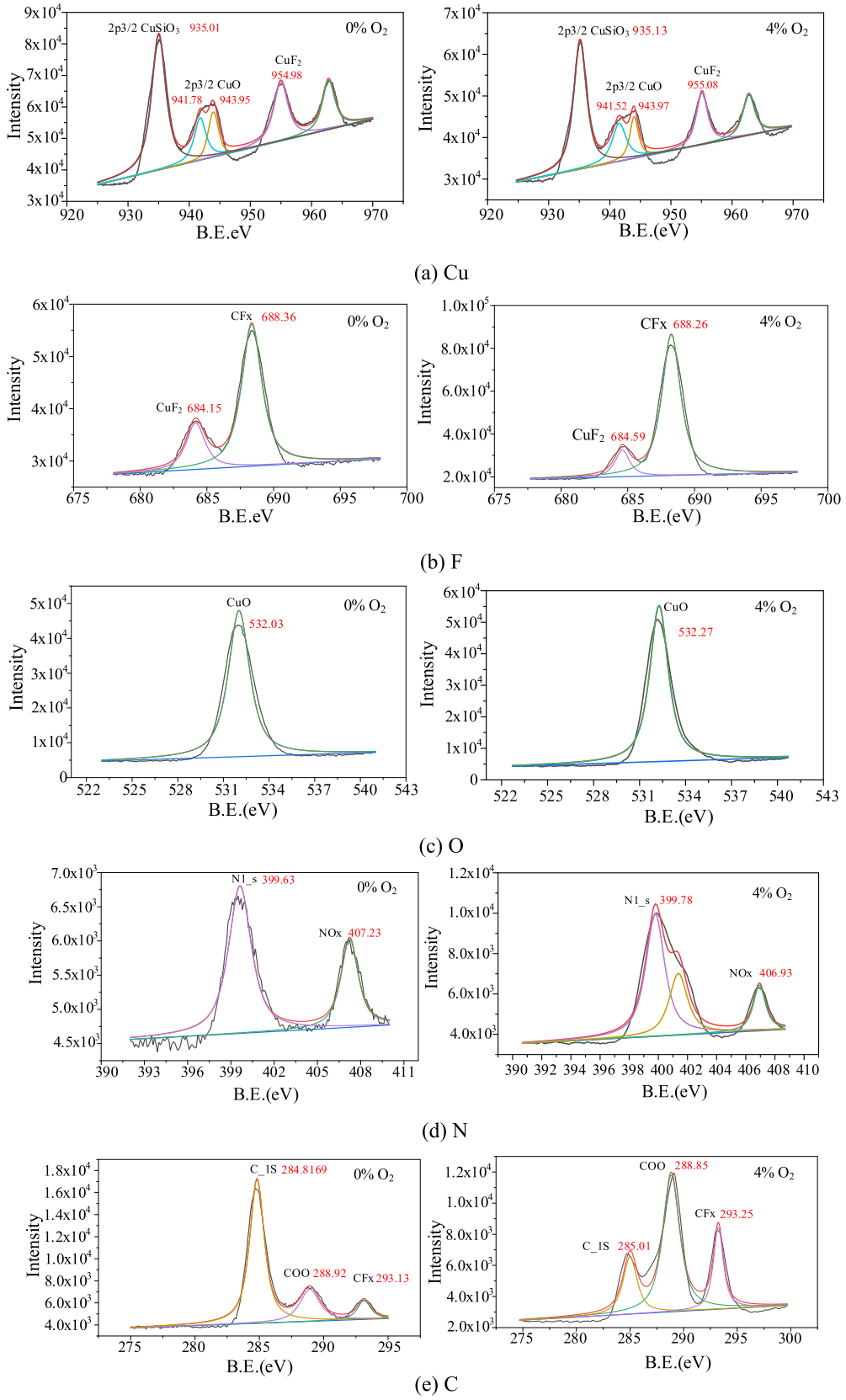

Figure 6. Analysis of XPS on the electrode surface after PD. (a) Cu. (b) F. (c) O. (d) N. (e) C.

and CFx (fluoride), respectively (Figure 6b). The characteristic peak of the O element at 532.02 eV corresponds to CuO (Figure 6c). The N element is mainly composed of two characteristic peaks at 399.63 and 407.23 eV, respectively, corresponding to N1_S and NOx (nitrogen oxides) (Figure 6d). The three characteristic peaks of element C at 284.81, 288.92, and 293.13 eV correspond to C_1S, O−C═O, and CFx (Figure 6e).

https://doi.org/10.1021/acsomega.3c00345
ACS Omega 2023, 8, 23457−23464

It can be seen that the substances corresponding to different characteristic peaks after adding 4% O_2 are basically the same as those without adding O_2, that is to say, the addition of O_2 will not have a significant impact on the composition of solid byproducts, which is mainly reflected in the difference in the content of components. It can be seen from the characteristic peak intensity that the content of O−C═O is significantly higher than that of CF_X and C under the condition of 4% O_2_1S, indicating that the amount of carbon and oxygen compounds in the byproducts increases after the addition of O_2. In general, the main substances causing electrode surface corrosion after the 96 h PD test of the C_4F_7N−CO_2−O_2 gas mixture include metal oxides (CuO), silicates ($CuSiO_3$), fluorides (CuF, CF_X), carbon oxides (CO, CO_2), and nitrogen oxides (NO, NO_2).

3.3. Discussion. *3.3.1. Formation Mechanism of Solid Byproducts of the C_4F_7N−CO_2−O_2 Gas Mixture.* In this paper, a pin-plate electrode model is used to carry out the PD decomposition test in a stainless-steel tank (gas chamber). The whole test model can be divided into three areas, including the main gas chamber area, the ion diffusion area, and the glow discharge area. The glow discharge area is located near the needle electrode. The electric field intensity in this area is high, and a large number of high-energy electrons will be generated during the discharge process; the resulting collision ionization process will lead to the dissociation and composite reaction of the C_4F_7N−CO_2−O_2 gas mixture to generate more gas and solid byproducts. The gas byproducts will uniformly diffuse into the stainless-steel gas chamber, and the solid byproducts will adhere to the electrode surface due to gravity. The projection of the electric field distribution of the needle-plate electrode on the plate electrode is circular, so the surface of the plate electrode will produce circular solid precipitates. The closer the distance to the tip of the needle electrode, the higher the electric field intensity, the stronger the collision ionization, and the more the byproducts generated, and so the darker the color of the solid precipitates in the area near the center of the plate electrode.

The solid byproducts are mainly formed by the interaction of the C_4F_7N gas mixture and its decomposition products with the brass metal electrode under the action of PD. The C_4F_7N−CO_2−O_2 gas mixture will decompose under the action of PD to generate particles with relatively active chemical properties such as F, O, and CN. These particles will interact with the copper electrode under the action of PD and generate solid precipitates on the electrode surface. Through XPS element valence analysis, it is found that Cu is mainly composed of three characteristic peaks located at 935.01, 943.95, and 954 eV, corresponding to $CuSiO_3$ $2p_{3/2}$, CuO $2p_{3/2}$, and CuF, which are the main sources of solid byproducts. Table 2 shows the generation paths of these main solid byproducts. CuF mainly comes from the interaction between F particles (generated by the decomposition of C_4F_7N) and Cu. CuO mainly comes from the interaction between O particles (generated by the decomposition of CO_2 and O_2) and Cu. $CuSiO_3$ mainly comes from the interaction between SiO_2 (generated by the observation window of the stainless-steel gas chamber) and Cu under the participation of O particles. Because the observation window is not designed in the actual equipment, $CuSiO_3$ generally does not appear during operation.

Table 2. Generation Path of Solid Byproducts

byproducts	reaction path
CuF	Cu + F → CuF
CuO	Cu + O → CuO
$CuSiO_3$	Cu + SiO_2 + O → $CuSiO_3$

3.3.2. Effect of O_2 on the Generation of Solid Byproducts and Application Suggestion. It can be seen that fluoride and oxide play a leading role in solid byproducts. Among them, oxides mainly come from O_2 and O particles participating in the reaction. The decomposition of background gas CO_2 will generate O particles, and the added gas O_2 may lead to the oxidation of metal conductors. Therefore, whether or not adding a certain amount of O_2 into the C_4F_7N−CO_2 gas mixture will aggravate the corrosion of metal conductors under PD fault needs further analysis.

From the microscopic morphology of solid byproducts, it can be seen from the distribution area and density of solid substances that the yield of solid products without O_2 is significantly greater than that with O_2. According to the quantitative analysis of gas decomposition products, the addition of 4% O_2 can significantly inhibit the formation of most fluorocarbon compounds. The content of the F element decreased significantly after the addition of O_2 according to the quantitative analysis of EDS given in Table 1, mainly due to the combination of some fluorocarbon compounds and O_2 to generate COF_2. The addition of O_2 can effectively inhibit the generation of some solid byproducts but also generate some harmful gas byproducts, such as COF_2 and CO, so the amount of O_2 addition should be strictly controlled while meeting the insulation and decomposition characteristics in the actual equipment. Previous research indicates that the gas−solid interface compatibility between the C_4F_7N−CO_2 gas mixture and copper is poor, and the surface of the copper sheet will be corroded when the interface temperature reaches above 170 °C.[22,23] It can be seen that compared with the corrosive effect of C_4F_7N on the metal, the addition of O_2 can also inhibit the generation of solid byproducts under the action of PD to a certain extent and reduce the corrosive effect of the C_4F_7N gas mixture on metal conductors.

During the operation of the C_4F_7N−CO_2−O_2 gas mixture GIE, it is necessary to try to avoid the adverse effects of solid byproducts generated by long-term PD fault decomposition on metal conductors and insulating parts in the equipment. On the one hand, solid precipitates attached to the metal conductor surface will change the electric field distribution around the conductor and then cause PD and even breakdown fault. In addition, solid precipitates may attach to the insulating parts inside the equipment, and the conductive components contained in these solid precipitates will affect its insulation performance, resulting in a series of insulation failures of the equipment. Therefore, it is necessary to monitor the PD failure inside the equipment in real time to avoid the impact of solid products generated by long-term discharge and serious failure on the safe and stable operation of the equipment. In addition, considering the corrosive effect of the C_4F_7N gas mixture on metal conductor copper under long-term PD fault, silver plating on a copper surface can solve this problem.

4. CONCLUSIONS

This paper studies the generation characteristics of solid byproducts of the C_4F_7N−CO_2−O_2 gas mixture under long-term PD fault, evaluates the compatibility of the C_4F_7N−

https://doi.org/10.1021/acsomega.3c00345
ACS Omega 2023, 8, 23457−23464

CO_2−O_2 gas mixture with a metal conductor under PD action, and gives application suggestions. The relevant conclusions are as follows.

(1) After the 96 h PD decomposition test, the C4F7N−CO2−O2 gas mixture showed obvious annular solid precipitates in the central area of the electrode surface, mainly composed of irregular crystal corrosion.
(2) The solid byproducts are mainly composed of five elements: Cu, F, O, N, and C. After adding 4% O_2 into the C_4F_7N−CO_2 gas mixture, the content of F decreases by 26.3%. The addition of O_2 has little effect on the element composition and valence of PD solid precipitates, which is mainly reflected in the difference in the component content.
(3) According to the element valence analysis, the solid byproducts on the electrode surface mainly include metal oxides (CuO), silicates ($CuSiO_3$), fluorides (CuF, CF_X), carbon oxides (CO, CO_2), and nitrogen oxides (NO, NO_2). Compared with the corrosive effect of C_4F_7N on metal, the addition of O_2 can inhibit the formation of solid precipitates under the action of the C_4F_7N mixture PD to a certain extent and reduce the corrosive effect of the C_4F_7N mixture on metal conductors.

AUTHOR INFORMATION

Corresponding Author

Dibo Wang − *Electric Power Research Institute, China Southern Power Grid, Guangzhou 510623, China; National Engineering Research Center of UHV Technology and New Electrical Equipment Fundamentals, Guangzhou 510623, China; United Laboratory of Advanced Electrical Materials and Equipment Support Technology, China Southern Power Grid, Guangzhou 510623, China;* orcid.org/0000-0002-1105-6339; Email: wangdibo@sina.com

Authors

Ran Zhuo − *Electric Power Research Institute, China Southern Power Grid, Guangzhou 510623, China; National Engineering Research Center of UHV Technology and New Electrical Equipment Fundamentals, Guangzhou 510623, China; United Laboratory of Advanced Electrical Materials and Equipment Support Technology, China Southern Power Grid, Guangzhou 510623, China*

Mingli Fu − *Electric Power Research Institute, China Southern Power Grid, Guangzhou 510623, China; National Engineering Research Center of UHV Technology and New Electrical Equipment Fundamentals, Guangzhou 510623, China; United Laboratory of Advanced Electrical Materials and Equipment Support Technology, China Southern Power Grid, Guangzhou 510623, China*

Yan Luo − *Electric Power Research Institute, China Southern Power Grid, Guangzhou 510623, China; National Engineering Research Center of UHV Technology and New Electrical Equipment Fundamentals, Guangzhou 510623, China; United Laboratory of Advanced Electrical Materials and Equipment Support Technology, China Southern Power Grid, Guangzhou 510623, China*

Guoli Wang − *Electric Power Research Institute, China Southern Power Grid, Guangzhou 510623, China; National Engineering Research Center of UHV Technology and New Electrical Equipment Fundamentals, Guangzhou 510623, China; United Laboratory of Advanced Electrical Materials and Equipment Support Technology, China Southern Power Grid, Guangzhou 510623, China*

Lei Jia − *Electric Power Research Institute, China Southern Power Grid, Guangzhou 510623, China; National Engineering Research Center of UHV Technology and New Electrical Equipment Fundamentals, Guangzhou 510623, China; United Laboratory of Advanced Electrical Materials and Equipment Support Technology, China Southern Power Grid, Guangzhou 510623, China*

Complete contact information is available at: https://pubs.acs.org/10.1021/acsomega.3c00345

Notes

The authors declare no competing financial interest.

ACKNOWLEDGMENTS

This work was supported by the science and technology project of China Southern Power Grid (Grant numbers YNKJXM20222118, YNKJXM20222131, YNKJXM20222043).

REFERENCES

(1) Zeng, F.; Wu, S.; Lei, Z.; Li, C.; Tang, J.; Yao, Q.; Miao, Y. SF_6 fault decomposition feature component extraction and triangle fault diagnosis method. *IEEE Trans. Dielectr. Electr. Insul.* **2020**, *27*, 581−589.

(2) Zhang, X.; Tian, Y.; Cui, Z.; Tang, J. Plasma-assisted abatement of SF_6 in a packed bed plasma reactor: understanding the effect of gas composition. *Plasma Sci. Technol.* **2020**, *22*, No. 055502.

(3) Xiao, S.; Shi, S.; Li, Y.; Ye, F.; Li, Y.; Tian, S.; Zhang, X. Review on decomposition characteristics of eco-friendly gas insulating medium for high voltage gas insulated equipment. *J. Phys. D: Appl. Phys.* **2021**, *54*, No. 373002.

(4) Tu, Y.; Chen, G.; Wang, C.; Shao, Y.; Tong, Y.; Li, C.; Ma, G.; Shahsavarian, T. Feasibility of C_3F_7CN/CO_2 gas mixtures in high-voltage DC GIL: a review on recent advances. *High Voltage* **2020**, *5*, 377−386.

(5) Xiao, S.; Gao, B.; Pang, X.; Zhang, X.; Li, Y.; Tian, S.; Tang, J.; Luo, Y. The sensitivity of C_4F_7N to electric field and its influence to environment-friendly insulati ng gas mixture C_4F_7N/CO_2. *J. Phys. D: Appl. Phys.* **2021**, *54*, No. 055501.

(6) Ye, F.; Zhang, X.; Xie, C.; Sun, X.; Wu, P.; Xiao, S.; Tang, J.; Li, Y. Effect of oxygen and temperature on thermal decomposition characteristics of $C_4F_7N/CO_2/O_2$ gas mixture for MV equipment. *IEEE Access* **2020**, *8*, 221004−221012.

(7) Yang, Y.; Gao, K.; Bi, J.; Ding, L.; Yuan, S.; Wang, G. Influence of micro-water on AC breakdown characteristics of C_4F_7N/CO_2 gas mixture under non-uniform electric field. *High Voltage* **2022**, *7*, 1059−1068.

(8) Toigo, C.; Vu-Cong, T.; Jacquier, F.; Girodet, A. Partial discharge behavior of protrusion on high voltage conductor in GIS/GIL under high voltage direct current: Comparison of SF_6 and SF_6 alternative gases. *IEEE Trans. Dielectr. Electr. Insul.* **2020**, *27*, 140−147.

(9) Song, J.; Li, X.; Zhang, Q.; Lv, Y.; Yuan, X.; Li, Z. Sensitivity of dielectric strength of C_4F_7N binary gas mixture to electric field distribution under lightning impulse. *IEEE Trans. Dielectr. Electr. Insul.* **2020**, *27*, 1152−1159.

(10) Wang, C.; Cheng, Y.; Tu, Y.; Chen, G.; Yuan, Z.; Xiao, A.; Owens, J.; Zhang, A. Characteristics of C_3F_7CN/CO_2 as an alternative to SF_6 in HVDC-GIL systems. *IEEE Trans. Dielectr. Electr. Insul.* **2018**, *25*, 1351−1356.

(11) Ye, F.; Zhang, X.; Li, Y.; Wan, Q.; Bauchire, J. M.; Hong, D.; Xiao, S.; Tang, J. Arc decomposition behavior of C_4F_7N/Air gas mixture and biosafety evaluation of its by-products. *High Voltage* **2022**, *7*, 856−865.

https://doi.org/10.1021/acsomega.3c00345
ACS Omega 2023, 8, 23457−23464

(12) Meyer, F.; Kieffel, Y. *Application of Fluoronitrile/CO2/O2 Mixtures in High Voltage Products to Lower the Environmental Footprint*; CIGRE Reports, 2018.
(13) Zhang, B.; Li, C.; Xiong, J.; Zhang, Z.; Li, X.; Deng, Y. Decomposition characteristics of C_4F_7N/CO_2 mixture under AC discharge breakdown. *AIP Adv.* **2019**, *9*, No. 115212.
(14) Li, Y.; Zhang, X.; Chen, Q.; Zhang, J.; Li, Y.; Xiao, S.; Tang, J. Influence of oxygen on dielectric and decomposition properties of C_4F_7N-N_2-O_2 mixture. *IEEE Trans. Dielectr. Electr. Insul.* **2019**, *26*, 1279−1286.
(15) Zhao, M.; Han, D.; Zhao, W.; Zhou, Z.; Zhang, G. Experimental and theoretical studies of C_3F_7CN/CO_2 mixture decomposition under overheating fault. *CSEE J. Power Energy Syst.* **2020**, *8*, 941−951.
(16) Li, Y.; Zhang, X.; Xiao, S.; Chen, Q.; Tang, J.; Chen, D.; Wang, D. Decomposition properties of C_4F_7N/N_2 gas mixture: an environmentally friendly gas to replace SF_6. *Ind. Eng. Chem. Res.* **2018**, *57*, 5173−5182.
(17) Wang, C.; Ai, X.; Zhang, Y.; Tu, Y.; Yan, X.; Liu, W. Decomposition products and formation path of C_3F_7CN/CO_2 mixture with suspended discharge. *IEEE Trans. Dielectr. Electr. Insul.* **2019**, *26*, 1949−1955.
(18) Zhao, M.; Han, D.; Zhou, Z.; Zhang, G. Experimental and theoretical analysis on decomposition and by-product formation process of $(CF_3)_2CFCN$ mixture. *AIP Adv.* **2019**, *9*, No. 105204.
(19) IEC-60270. High Voltage Test Techniques-Partial Discharge Measurements. 2000.
(20) Zhang, X.; Chen, Q.; Zhang, J.; et al. Experimental study on power frequency breakdown characteristics of C_4F_7N/CO_2 gas mixture under quasi-homogeneous electric field. *IEEE Access* **2019**, *7*, 19100−19108.
(21) Ye, F.; Zhang, X.; Li, Y.; Yao, Y.; Xiao, S.; Xie, C.; Sun, X.; et al. Effect of O_2 on AC partial discharge and decomposition behavior of $C_4F_7N/CO_2/O_2$ gas mixture. *IEEE Trans. Dielectr. Electr. Insul.* **2021**, *28*, 1440−1448.
(22) Li, Y.; Zhang, X.; Chen, Q.; Zhang, J.; Chen, D.; Cui, Z.; Xiao, S.; Tang, J. Study on the Thermal Interaction Mechanism between C_4F_7N-N_2 and Copper, Aluminum. *Corros. Sci.* **2019**, *153*, 32−46.
(23) Li, Y.; Zhang, X.; Xiao, S.; Chen, D.; Liu, C.; Shi, Y. Insights into the interaction between C_4F_7N decomposition products and Cu (1 1 1), Ag (1 1 1) surface. *J. Fluorine Chem.* **2018**, *213*, 24−30.

https://doi.org/10.1021/acsomega.3c00345
ACS Omega 2023, 8, 23457−23464